Compressive Behavior of Concrete-Filled Filament-Wound FRP Tubes with Local Tube Damage

Guan LIN[1] and Yu XIANG[2]*

ABSTRACT

Concrete-filled fiber-reinforced polymer (FRP) tubes (CFFTs) are an emerging and attractive form of columns for new construction. Such a column typically consists of an outer filament wound FRP tube filled with plain or steel reinforced concrete. The fibers in the filament wound FRP tube are predominantly in the hoop direction to confine the inner concrete, leading to significantly enhanced strength and ductility for the confined concrete. Extensive studies have been conducted on the behavior of CFFTs subjected to various loading conditions, confirming the excellent performance of such members. As CFFTs become more and more widely used in practice, one concern remains regarding the performance of CFFTs when the FRP tube is subjected to local damage caused by accidents, vandalism, or designed holes or cuts to accommodate connection with other structural components. Although there have been some existing studies on the performance of CFFTs as flexural members with a locally damaged filament wound FRP tube, the research on such CFFTs as columns remains limited. This paper therefore presents the results of a comprehensive experimental program on the axial compressive behavior of CFFTs with a filament wound FRP tube subjected to local tube damage. Two types

[1] Assistant Professor, Department of Ocean Science and Engineering, Southern University of Science and Technology, Shenzhen, Guangdong 518055, China; Former Research Assistant Professor, Department of Civil and Environmental Engineering, The Hong Kong Polytechnic University, Hong Kong, China. (ling@sustech.edu.cn)

[2] Research Assistant Professor, Department of Civil and Environmental Engineering, The Hong Kong Polytechnic University, Hong Kong, China. (**Corresponding author:** cee.yu.xiang@polyu.edu.hk)

of damage (i.e., holes and cuts) with different parameters were investigated. The test results showed that the compressive strength and the corresponding axial strain of the damaged CFFTs were significantly reduced due to the local tube damage (the compressive strength reduced from 12.2% to 64.8% and the corresponding axial strain reduced from 35.2% to 77.2%). Finally, an existing model for FRP-confined concrete considering the local FRP damage was evaluated using the test results of the presents study, suggesting the need for re-calibration of the model or the development of a new model for CFFTs with a locally damaged filament FRP tube.

Keywords: Fiber-reinforced Polymer (FRP); Filament-wound FRP Tubes; Confinement; Local Damage; Compressive Behavior.

INTRODUCTION

Concrete-filled fiber-reinforced polymer (FRP) tubes (CFFTs) (Mirmiran and Shahawy 1997; Fam and Rizkalla 2001a,b; Zhang *et al.* 2015; Dong *et al.* 2021) are an emerging and attractive form of columns for new construction, which consists of an outer FRP tube filled with plain or steel reinforced concrete. FRP tubes manufactured through a filament-winding process are typically used in CFFTs. The fibers in the filament wound FRP tubes are predominantly in the hoop direction to confine the inner concrete that dilates under axial compression. The lateral confinement provided by the FRP tube can significantly enhance both the strength and the ductility of the confined concrete, leading to a highly ductile compressive behavior for the member formed from two brittle materials (i.e., concrete and FRP). In addition to the excellent mechanical performance, CFFTs also possess excellent corrosion resistance and high strength-to-weight ratios compared with columns with other conventional materials (e.g., steel). With these advantages, CFFTs are attractive for use as structural components exposed to harsh outdoor environments (e.g., bridge columns and marine piles).

Over recent years, extensive studies have been conducted on CFFTs as flexural members or compressive members. Different behavioral aspects of CFFTs have been investigated, including their monotonic axial compressive behavior (e.g., Mirmiran and Shahawy 1997; Fam and Rizkalla 2001a,b; Ozbakkaloglu and Oehlers 2008; ElGawady and Dawood 2012; Gholampour and Ozbakkaloglu 2018), cyclic axial compression behavior (e.g., Yu *et al.* 2015; Zhang *et al.* 2015), flexural behavior (e.g., Burgueño and Bhide 2006; Shi *et al.* 2011), seismic behavior (e.g., Zhu *et al.* 2006; Zohrevand and Mirmiran 2013), blast resistance behavior (e.g., Qasrawi *et al.* 2015), durability performance (e.g., Robert and Fam 2012; El-Zefzafy *et al.* 2013; Wang and

55 ElGawady 2020), fire resistance performance (e.g., Ji *et al.* 2008; Echevarria *et al.* 2015), as well
56 as design methods (e.g., Yu and Teng 2011; AASHTO 2012). The existing studies have
57 generally confirmed the excellent mechanical and durability behavior of CFFTs.
58
59 As CFFTs have become more and more widely used in practice (e.g., Fam *et al.* 2003a; Fam *et al.*
60 2003b; Jawdhari *et al.* 2020; Adheem *et al*. 2021) and considering that the FRP tube in a CFFT is
61 directly exposed, one concern remains regarding the performance of CFFTs subjected to local
62 tube damage. The local damage of the FRP tube may arise due to two major reasons: (1)
63 accidental damage or vandalism caused by car, ship, or debris impact, or sharp tools (e.g., axes,
64 saws, or knives); (2) pre-drilled holes or designed cut(s) to accommodate connection with other
65 structural components (e.g., beams, braces). For the latter, the use of bolts for beam-column
66 connections often requires pre-drilling of holes through the thickness of the FRP tubes. The
67 connection of a steel section with the CFFT also requires horizontal and/or vertical cut(s) to
68 allow the steel section to go through. The vulnerability of CFFTs to the above accidental or
69 designed damage has been little studied. Particularly, the behavior of CFFTs as columns with a
70 filament wound FRP tube subjected to local tube damage has not been investigated in detail.
71
72 Lu *et al.* (2020) was the first to investigate experimentally the effect of local FRP tube damage
73 on the flexural behavior of CFFTs in four-point bending. In their study, FRP tubes with a near-
74 cross-ply laminate structure (the fibers were predominately in the longitudinal and hoop direction)
75 were used. The test results revealed that a cut in the hoop direction were the most critical type of
76 damage for the flexural behavior of CFFTs. A hoop cut of 20% of the perimeter on the tension
77 side reduced the flexural strength by 75%. Lu and Fam (2020) later investigated the effect of

78 local damage of filament wound FRP tubes with a fiber angle of ±55° on the flexural behavior of
79 CFFTs in four-point bending. They found that the CFFTs with such angle-ply FRP tubes were
80 less vulnerable than those with near-cross-ply FRP tubes in their previous study: a hoop cut of 10%
81 of the perimeter on the tension side led to a flexural strength reduction of 31%. Based on the
82 results of the above experimental studies as well as finite element (FE) modelling, Jawdhari *et al.*
83 (2021a) proposed a design equation for the flexural strength of CFFTs with local tube damage,
84 with the effects of cut length, diameter-to-thickness ratio, and type of laminate structure of the
85 FRP tube taken into consideration. Jawdhari *et al.* (2021b) conducted an FE modelling study on
86 the behavior of FRP-wrapped circular concrete columns subjected to local damage of the FRP
87 wrap. The FRP wraps were formed via the wet lay-up method with fibers oriented only in the
88 column hoop direction. The effects of cut orientation, cut length, cut location, diameter-to-jacket
89 thickness ratio on the behavior of such columns were investigated. Based on the results of a
90 parametric study using the FE model, a confinement stress-strain model of FRP-confined
91 concrete considering the local damage of the FRP wrap was proposed. However, the FE model in
92 their study was mainly verified using test results of FRP-confined concrete cylinders with intact
93 FRP wraps collected from the literature. In addition, as the considered FRP wraps had fibers only
94 in the hoop direction, the effects of hoop cut on the behavior of FRP-wrapped concrete columns
95 were found to be negligible as expected.
96
97 In practice, CFFTs with filament wound FRP tubes are more desirable than those with FRP
98 wraps with fibers only in the hoop direction, as the filament wound FRP tube can serve directly
99 as the formwork for casting concrete. In addition, the filament winding process results in FRP
100 tubes with a sufficient longitudinal stiffness in resisting the constructional and service loadings

to avoid cracking of the FRP tube, leading to high durability of the structure. The effect of local tube damage on the compressive behavior of CFFTs is rarely explored. To the best of the authors' acknowledgement, only two studies have been conducted on CFFT columns with local tube damage (Tejada 2021; Taveras *et al.* 2022). Tejada (2021) investigated the effects of linear cuts in vertical, diagonal and horizontal directions on the compressive behavior of CFFTs. It was found that the linear cuts significantly affected the stress-strain behavior of CFFTs beyond the level of unconfined concrete strain and a vertical or diagonal cut was more critical than a horizontal cut on the compressive strength of CFFTs. Taveras *et al.* (2022) focused on the effects of linear cuts on the axial strength of CFFTs; they also found that horizontal cuts had an insignificant effect on the axial strength of CFFTs. Obviously, more research is needed to allow a clear and in-depth understanding of the behavior of CFFTs with local tube damage to be obtained. Against this background, a comprehensive experimental program was carried out in the present study, and the test results are presented in this paper. Two different types of damage (i.e., holes and cuts) were included to simulate the different types of damage in practice. For the damage of holes, the effects of hole number, hole size, and hole distance were investigated, while for the damage of cuts, the effects of cut direction and cut length were investigated. The present experimental study provided the much-needed experimental data for the future FE modelling and the development of design methods for CFFTs as columns with local FRP tube damage. In the present paper, compressive stresses/strains in concrete are defined to be positive while tensile stresses/strains in FRP tubes are defined to be positive.

EXPERIMENTAL PROGRAM

Specimen Details

A total of 24 CFFT specimens with a diameter of 150 mm and a length of 300 mm for the concrete core were prepared and tested under axial compression, which are divided into three groups. Group A included two nominally identical CFFT specimens without tube damage, Group B included 10 CFFT specimens with tube damage induced by cutting, and Group C included 14 CFFT specimens with tube damage induced by drilling holes (Figure 1). In Group B, each CFFT specimen possessed a vertical or horizontal cut at the mid-height of the specimen; the cut orientation and the cut length were the main test variables (Figure 1b). In Group C, each CFFT specimen possessed drilling holes largely at the mid-height of the specimen; the diameter, number, vertical and horizontal distances between holes were the main test variables (Figure 1c). Each specimen was given a name. For each specimen in Group B, the name starts with "C" denoting the damage of cut, followed by an underline and "hx" or "vx" representing a horizontal or a vertical cut with a length of x mm. For each specimen in Group C, the name starts with "H" denoting the damage of hole(s), followed by an underline and "nx_1dy_1" representing the number (of x_1) and the diameter (of y_1 mm) of the hole(s); the following "vx_2hy_2" represents the vertical center-to-center distance (of x_2 mm) and the horizontal center-to-center distance (of y_2 mm) between the holes. All the names end with "1" or "2" to differentiate two nominally identical specimens. The details of the test specimens are listed in Table 1. Prefabricated filament wound glass FRP (GFRP) tubes with a nominal fiber thickness of 2.3 mm were used for all specimens. The tubes were manufactured using E-glass fibers and viny ester resin, with the fibers being arranged at ±80° to the longitudinal axis.

Fabrication of Specimens

The filament wound FRP tubes fixed on wooden plates using steel rods were directly used as the

147 formwork for casting concrete. The CFFT specimens were cured in the ambient environment of
148 the laboratory for at least 52 days. After the curing of concrete, each end of the specimen was
149 strengthened with an additional 25-mm-width CFRP strip to avoid unexpected failure near the
150 two ends. The two end surfaces of each specimen were capped with high-strength gypsum to
151 ensure a flat and smooth condition for receiving axial load. Local damage was then induced in
152 the FRP tube before the testing of the CFFT specimens. The cut damage of the FRP tube was
153 achieved using a precise cutting machine (Figure 2a), while the holes were made by a drilling
154 machine with a desired diameter for the drilling head (Figure 2b). The machine used for cutting
155 was a corded multi-functional cutting tool with a capacity of 130 W and a maximum rotary speed
156 of 33,000 RPM. A cordless cutting tool with a lower capacity of 64 W and a maximum rotary
157 speed of 28,000 RPM was used instead for drilling holes with a diameter of 5 mm or 8 mm; a
158 drilling head of a double cut carbide burr with a cutting diameter of 3 mm was used for drilling
159 the holes. Both machines were precisely controlled to ensure that the cuts and the holes went
160 through the thickness of the FRP tube, but the inner concrete was little damaged.
161
162 **Material Properties**
163 *Concrete*
164 The concrete had a target compressive strength of 30 MPa and the raw materials included ASTM
165 Type I Portland cement, river sand, fly ash, granite coarse aggregate with a maximum nominal
166 diameter of 10 mm, and superplasticizer (S.P.). Three standard plain concrete cylinders (diameter
167 × height = 150 mm × 305 mm) were cast and tested under axial compression to obtain the
168 concrete properties. The average compressive strength, axial strain at peak stress, and elastic
169 modulus were measured to be 31.0 MPa, 0.262%, and 22.8 GPa, respectively. These standard

concrete cylinders were tested one day before the compression tests on CFFT columns; the latter lasted for around three days.

Filament wound FRP tubes

The filament wound FRP tube had fibers oriented close to the tube hoop direction (i.e., ±80°), and thus the hoop properties are of importance to understanding the mechanical behavior of CFFTs. To obtain the hoop tensile properties of the FRP tubes, tensile split-disk tests on four FRP rings with a uniform height of 35 mm cut from an FRP tube of the same batch as those used in the CFFTs were conducted following ASTM D2290 (2019). Four hoop strain gauges with a gauge length of 20 mm were attached on the outer surface of each FRP ring. The four hoop strain gauges were attached 15 mm away from the gaps of the split disk and the readings were averaged to obtain the ultimate strength, rupture strain and the secant elastic modulus of the FRP tubes at rupture, which were 687.3 MPa, 1.71% and 40.2 GPa, respectively, based on a nominal fiber thickness of 2.3 mm. Figure 3 shows the hoop stress-hoop strain curves of the test FRP rings, which generally exhibit a linear elastic behaviour due to the fibres close to the tube hoop direction.

Instrumentation and Test Procedure

Figure 4 shows the test set-up and the instrumentation of the test CFFTs. For each CFFT specimen, eight hoop strain gauges with a gauge length of 20 mm were evenly installed around the circumference of the mid-height section to monitor the hoop strains, with one of them being installed near the cut or the hole (when a cut or a hole existed at the mid-height section) or at the center between the two holes or two rows of holes (when a cut or a hole did not exist at the mid-

height section) (Figure 4a). In addition, four axial strain gauges with a gauge length of 20 mm were installed at 90° apart at the mid-height section to monitor the axial strains (with one of them being installed near the cut or the hole) (Figure 4a). Two linear variable differential transformers (LVDTs) covering a mid-height length of 150 mm (referred to as the mid-height LVDTs) were installed at 180° apart on the FRP tube to monitor the axial strains near the mid-height. The two LVDTs were attached to the FRP tube using epoxy mortar to avoid any local damage to the FRP tube (Figure 4b). In addition to the two mid-height LVDTs, four LVDTs were installed between the top and bottom loading plate to monitor the full length shortening of the specimen (referred to as the full-height LVDTs).

The axial compression tests were performed using an MTS machine with a loading capacity of 4500 kN. Each specimen was compressed with a displacement control rate of 0.18 mm/min. The axial load was applied on both the FRP tube and the inner concrete of each specimen. The readings of strain gauges, load cells, and LVDTs were recorded simultaneously by a data logging system.

EXPERIMENTAL RESULTS

Failure Mode

Figure 5 shows the typical failure process of the test specimens. Not all specimens are shown in the figure as the failure processes of some of them are similar. The failure of a control specimen (e.g., specimen Control_2) was initiated by the emerging of white patches along the fiber directions near the mid-height region, followed by explosive fiber fracture (Figure 5a) with a loud noise. The specimen with a horizontal cut (e.g., specimen C_h50_2) was characterized with

some small white patches near the cut during most of the loading process. The areas of white patches spread along the height of the specimen near the final failure of the specimen, accompanied by a loud noise. The total area of the white patches was smaller than those of the control specimen (Figure 5b) and the final rupture sound was also smaller.

The failure of a specimen with a vertical cut (e.g., specimen C_v50_2 or C_v150_2) was obviously different from that with a horizontal cut. For the specimen with a vertical cut of a relatively small length (specimens C_v50), the failure was initiated by outward buckling of the FRP tube near the cut, followed by fiber rupture in the fiber direction near the two ends of the cut, resulting in a large opening of the FRP tube near the vertical cut (Figure 5c). For the specimen with a vertical cut of a large length (specimens C_v150), buckling of the FRP tube occurred in the mid-height region, followed by horizontal cracks with fiber rupture near the two ends of the vertical cut. The opening of the FRP tube after failure was limited to the region of the vertical cut of the FRP tube (Figure 5d).

The failure of a specimen with holes initiated with the occurrence of “X-shaped” white patches around the holes. Fiber rupture occurred near the holes and gradually developed to “X-shaped” cracks around the holes, followed by a sudden final rupture near the holes (Figures 5e to 5j). The sound of the final rupture, however, was much lower than that of the control specimens. For the specimen with holes of a large distance (e.g., specimen H_n2d8_150h0_2), the final fiber rupture occurred near the holes, as well as in the mid-height region without tube damage (Figure 5g). In comparison to a control specimen, a specimen with holes failed with a more localized pattern, as indicated by much smaller areas of fiber rupture in the FRP tube. Comparing specimens with

holes of different diameters (specimen H_n2d5_v50h0_1 versus specimen H_n2d8_v50h0_1), the fiber rupture zone of the specimen with smaller diameter holes was more focused near the mid-height region.

Stress-Strain Curves

Figure 6 depicts typical experimental axial load-strain curves from two test specimens with (i.e., specimen C_v50_1) and without (i.e., specimen Control_2) tube damage, respectively. The axial strains obtained by averaging the outputs of four axial strain gauges (referred to as the average SG axial strain) and those obtained from specimen shortenings measured by LVDTs (referred to as the nominal axial strain) for a specimen without tube damage are compared in Figure 6a. It is seen that, at a given axial load, the average SG axial strain is in good agreement with the nominal axial strains when the strain is lower than around 2%, beyond which the nominal strain becomes increasingly larger than the average SG strain. The smaller average SG axial strains than the nominal axial strains are also reported in Zhang *et al*. (2017), which they believed was attributed to the slips between the concrete and the FRP tube during a later loading stage. In addition, local damage due to fiber rupture did not always occur exactly at the mid-height of the specimen where the strain gauges were installed; therefore, larger axial strains due to such local damage could not be captured by the strain gauges installed at the mid-height. Figure 6a also shows that the FRP hoop strains around the perimeter are close to each except for some strain fluctuations during the later loading stage.

For a specimen with local tube damage (Figure 6b), the axial strain gauge readings exhibited larger non-uniformity than those of the specimen without tube damage, and the average SG axial

262 strains are smaller than the nominal axial strains when the axial strains are lower than around 1%.
263 Shortly after the peak axial load, the nominal axial strain continued to increase while the
264 magnitudes of both the average SG axial strain and the average hoop strain started to reduce due
265 to localized failure near the tube damage resulting in unloading in the axial and hoop directions
266 of the FRP tube far away from the damage. As a result, the nominal axial strains obtained from
267 LVDTs may be more reasonable to represent the average axial behavior of a CFFT specimen
268 with local tube damage. Figure 6b further shows that for both specimens with and without tube
269 damage, the nominal axial strains obtained from the full-height LVDTs are generally very close
270 to those from the mid-height LVDTs throughout the loading process. The axial load-strain curve
271 obtained with the former is shown to be more stable at the post-peak descending branch (Figure
272 6b). Therefore, the axial strains obtained from the full-height LVDTs are used in the subsequent
273 discussion of the test results of all CFFT specimens in the present paper
274
275 Figure 7 shows the axial stress-axial strain curves of all CFFT specimens. The axial stresses were
276 obtained from the recorded axial loads divided by the cross-sectional area of the confined
277 concrete. It is evident that the axial stress-axial strain curve of a CFFT specimen without local
278 tube damage features a typically bilinear shape before a sudden load drop caused by FRP tube
279 rupture (Figure 7a). The axial stress-axial strain curve of a CFFT specimen with local tube
280 damage induced by a horizontal cut (Figures 7b) or holes (Figures 7f to 7l) also features a
281 bilinear shape before the peak stress, followed by a sudden axial stress drop due to FRP rupture
282 with a descending branch. The axial strain at peak axial stress varies with the level (i.e., number
283 of holes) or the characteristics (e.g., cut or distance of holes) of damage in the FRP tube. For the
284 specimen with a relatively small vertical cut (e.g., specimens C_v50, Figure 7c), the axial stress-

axial strain curve still features a bilinear shape; however, as the length of the cut increases, the axial stress-axial strain curve becomes more similar to that of unconfined concrete, with the peak axial stress being closer to the unconfined concrete strength and the descending branch being less steep (Figures 7d and 7e), an indicator of a smaller confinement provided by the FRP tube. It should be noted that the test curve of specimen C_v100_1 (Figure 7d) is unreliable due to an operational error during the test and thus the test results of this specimen are excluded in the subsequent discussions of the present paper.

Ultimate Conditions

Table 2 summarizes the key test results of all CFFT specimens, including the compressive strength (i.e., peak stress) (f'_{cc}), the axial strain at peak stress (ε_{cc}), the ultimate axial strain (ε_{cu}), and the average FRP hoop rupture strain ($\varepsilon_{h,rup}$). The ultimate axial strain (ε_{cu}) is defined as the point when a 15% reduction in axial stress is achieved after the peak stress. Obviously, for a specimen with an abrupt axial stress reduction after the peak, the value of ε_{cu} is very close to that of ε_{cc}; however, for a specimen with a gradual descending branch after the peak stress, the value of ε_{cu} is larger. It should be noted that, for intact CFFT specimens and most CFFT specimens with local tube damage, obvious FRP tube rupture occurred at the peak stress; however, for some CFFT specimens with large cut in the FRP tube (e.g., specimens C_v100 and C_v150), fiber rupture occurred early (before the peak stress) near the two ends of the cut without obvious tube rupture (Figure 5d). For the latter specimens, the average FRP hoop strains at peak stress are listed in Table 2 for the FRP hoop rupture strain ($\varepsilon_{h,rup}$). Table 2 shows that various forms of local tube damage reduced the compressive strength and the corresponding axial strain, which could be well-understood by the reduced confinement of FRP tube due to damage. The

reductions in the compressive strength and the corresponding axial strain of specimens with vertical cuts are larger than those with horizontal cuts. The reductions of specimens with damage induced by holes are influenced by the number, diameter, and distance of the holes. Due to the damage in the FRP tube, the average FRP hoop rupture strains ($\varepsilon_{h,rup}$) are also dramatically reduced. The reductions in FRP hoop rupture strain in specimens with a damage of cut are dramatically larger than those with damage of holes, which is consistent with the observation made on the compressive strength. This is reasonable as the lengths of the cut (50-150 mm) are much larger than the diameters (5-8 mm) of the holes.

DISCUSSION

Effect of Cutting Angle

Figure 8 compares the CFFT specimens with different cutting angles (i.e., a horizontal cut versus a vertical cut both with a length of 50 mm). As shown in Figure 8a, compared with the CFFT without tube damage in which the failure region (with white patches and fiber rupture) spread over almost the entire height of the specimen, the specimen with a horizontal cut of 50 mm (specimen C_h50) exhibited a similar failure pattern with more than one location of fiber rupture over the height of the specimen but with smaller areas of white patches. However, for the specimen with a vertical cut of 50 mm (specimen C-v50), failure concentrated near the cut at the mid-height of the specimen with other areas of the FRP tube remained almost intact. Since the FRP tubes in the present study possessed fiber angles of ±80° to the longitudinal axis, a vertical cut led to more fiber cutting than a horizontal cut with the same length. For a vertical cut of 50 mm, the projected cut length perpendicular to the fiber directions is 49.2 mm (i.e., $50 \times \sin|\pm 80°|$), whereas for a horizontal cut of 50 mm, the value reduces to 8.68 mm (i.e., $50 \times$

331 cos|±80°|).

332

333 Figure 8b shows the comparison of the average axial stress-axial strain curves of the three
334 specimens, and the compressive strengths and the ultimate axial strains are shown in Figures 8c
335 and 8d, respectively. The curve of unconfined concrete (i.e., plain concrete) is also shown in the
336 figure (labeled as "PC") for comparison. It is evident that the ultimate axial stress and axial strain
337 are both reduced due to the cut damage; the reductions in specimen C_v50 (44.0% in
338 compressive strength and 55.1% in ultimate axial strain) are much larger than those in specimen
339 C_h50 (12.2% in compressive strength and 35.1% in ultimate axial strain) (Figures 8c and 8d).
340 Before the peak axial stress, the axial stress-axial strain curves of both specimens generally
341 follow the curve of the specimen with intact FRP tube. Specimen C_h50 failed in a more sudden
342 manner than specimen C_v50 as indicated by a more sudden axial stress drop in specimen C_h50
343 which possessed a larger axial stress at failure. Specimen C_v50 failed in a more progressive
344 manner with a much more gradually descending branch after the peak axial stress.

345

346 **Effect of Vertical Cut Length**

347 Figure 9 compares the specimens with a vertical cut of different lengths (0, 50 mm, 100 mm, and
348 150 mm). The failure of the specimens with a vertical cut generally localized in the cut zone
349 (Figure 9a). Compared with specimen C_v150 in which the FRP tube opened exactly along the
350 cut length, some fiber rupture occurred outside the vertical cut zone in specimen C_v50 as shown
351 in Figure 9a. Figure 9b compares the average axial stress-axial strain curves of the specimens.
352 The compressive strength reduces significantly with the cut length. A vertical cut with a length
353 of 50 mm, 100 mm, and 150 mm led to a reduction of 44.0%, 61.3%, and 64.8%, respectively, in

compressive strength and a reduction of 55.1%, 49.2%, and 77.2%, respectively, in ultimate axial strain (Figures 9c and 9d, Table 2). Again, note that a vertical cut of 50 mm already led to a large reduction in the performance of CFFTs. The compressive strengths of specimens C_v100 and C_v150 are close to the compressive strength of unconfined concrete, indicating that the FRP tubes were seriously damaged by the vertical cut. However, compared with sudden failure of unconfined concrete, the axial stress-axial strain curves of the damaged CFFT specimens exhibit a more gradual descending branch due to the confinement of the intact FRP tube near the two column ends. Compared with specimen C_150 with a large vertical cut, specimen C_v100 possessed a more gradual descending branch.

Effect of Vertical Distance of Holes

Figure 10 shows the effect of distance of two holes (diameter = 8 mm) in the vertical direction of the FRP tube. When the distance of the two holes is relatively small (specimen H_n2d8_v50h0), fiber rupture initiated near the holes and spread near the damage zone, leading to a failure zone at the mid-height of the specimen (Figure 10a). When the distance is large (specimen H_n2d8_v150h0), fiber rupture occurred near the holes, as well as at the mid-height where the FRP tube was intact (Figure 10a). In terms of the axial stress-axial strain curve (Figure 10b), a larger distance of the two holes led to a slightly larger axial compressive strength. This is because a larger hole distance resulted in the holes farther away from the mid-height region where the concrete dilation is expected to be larger than that near the column ends. For specimen H_n2d8_v150h0 with the largest hole distance, the reductions in compressive strength and ultimate axial strains are 22.3% and 39.4%, respectively (Figures 10c and 10d). It can be seen that the strength and strain reductions in these specimens are generally smaller than those of

specimens with a vertical cut (Figure 9). As explained earlier, the two holes with a diameter of 8 mm generated a smaller area of fiber which was cut off by the holes than that by the vertical cuts.

The above observations cast doubt on the reliability of the technique of employing a test rig with screws for fixing LVDTs onto a CFFT. Such test rigs, which consist of a bottom ring and a top ring with tightening screws to firmly clamp the entire frame onto the column (Figure 11a) (ASTM C469 2022), have been widely used in the axial compression tests on CFFTs in previous studies (e.g., Teng *et al.* 2007; Vincent and Ozbakkaloglu 2013; Hassanli *et al.* 2020; Rodsin *et al.* 2020; Tijani *et al.* 2020). To firmly clamp the test rig onto the column, the sharp heads of screws may puncture the FRP tube and such damage may become more serious when concrete dilation becomes larger. Such damage on the FRP tube induced by screws may cause fiber rupture and thus a premature failure of the specimen. Figure 11b shows a typical failure mode of an CFFT installed with such a test rig under axial compression. It is seen that the failure mode is similar to that of specimen H_n2d8_v150h0 with two holes (Figure 5g) but differs from that of the control specimen without tube damage tested in the present study (see Figure 5a). Note that the LVDTs were attached to the FRP tube using epoxy mortar without screws in the present study (Figure 3b). The above comparison suggests that the compressive strength and the corresponding axial strain of a CFFT may be underestimated if a screw-type test rig is used for installation of LVDTs. Thus the method used in the present study (i.e., using epoxy mortar) (Zhang *et al.* 2017) is highly recommended for testing CFFTs. Nevertheless, it should be noted that the effect of such damage induced by screws may be affected by the fiber angles in the FRP tube. Further research is worthwhile for investigating the effect of local damage of FRP tubes with different fiber angles on the behavior of CFFTs.

400

401 **Effect of Horizontal Distance Between Two Columns of Holes**

402 Figure 12 illustrates the effect of horizontal center-to-center distance between two columns of
403 holes with a diameter of 8 mm. For specimen H_n2d8_v50h0, only one column of holes (i.e.,
404 two holes) were drilled, while two columns of holes (i.e., four holes) were drilled for the other
405 specimens. The failure modes of the three specimens are similar as shown in Figure 12a, in
406 which the failure of fiber rupture localized near the mid-height region with the holes. The three
407 specimens also exhibited very close axial stress-axial strain curves as shown in Figure 12b,
408 despite that specimen H_n2d8_v50h0 had only two holes while the remaining two specimens
409 had four holes. This implies that the horizontal distance between two columns of holes does not
410 have a significant effect on the behavior of CFFTs. The reductions in the compressive strength of
411 the three specimens compared with intact CFFTs are in the range of 26.7% to 30.3% and those in
412 the ultimate axial strain are in the range of 46.0% to 46.3%.

413

414 **Effect of Hole Diameter**

415 Figure 13 shows the effect of hole diameter by comparing the behaviors of two CFFT specimens
416 with different diameters of holes (vertical distance of the holes = 50 mm), as well as the intact
417 CFFT specimen. It is seen that the specimen with a hole diameter of 5 mm (specimen
418 H_n2d5_v50h0) possessed a more localized damage zone than the specimen with a hole
419 diameter of 8 mm (specimen H_n2d8_v50h0) (Figure 13a). The axial stress-axial strain curves of
420 the two specimens, including the descending branch after the peak stress, are close to each other.
421 Specimen H_n2d5_v50h0 possesses slightly larger compressive strength and ultimate axial strain,
422 which is reasonable as a smaller-diameter hole leads to a smaller area of fibers cut off by the

holes. The reduction in the compressive strength and ultimate axial strain of specimen H_n2d5_v50h0 are respectively 26.4% and 45.7%, which are already very large considering the small diameter of the holes (5 mm).

Effect of Hole Number

Figure 14 shows the effect of hole number on the behavior of CFFT columns. The hole diameter was 8 mm for all specimens. Specimen H_n2d8_v50h0 had two holes with a vertical center-to-center distance of 50 mm, specimen H_n3d8_v50h0 had three holes with a vertical distance of 25 mm, and specimen H_n4d8_v50h50 had two rows of holes (i.e., four holes) with a vertical and horizonal distance of 50 mm. Figure 14a shows that the failure modes of the three specimens with different numbers of holes are very close to each other and much more localized than the control specimen. Figures 14b-14d show that the axial stress-axial strain curves, including the compressive strengths and the ultimate axial strains, of the three specimens are also close to each other. However, it is expected that a larger reduction in performance may occur if the number of holes and the area covered by the holes further increase, as larger area of fibers will be cut off by the holes.

Effect of Damage Type

Obviously, the two different types of damage (i.e., cuts and holes) led to significantly different failure modes and stress-strain behaviors of CFFTs. This is mainly due to the different amount of fibers cut by the damage. As mentioned earlier, a vertical cut of 50 mm (specimens C_v50_1/2) led to a cut length of 49.2 mm perpendicular to the fiber direction and a horizontal cut of 50 mm (specimens C_h50_1/2) led to a cut length of 8.68 mm perpendicular to the fiber direction. For

446 the damage induced by drilling holes, the cut length perpendicular to the fiber direction is equal
447 to the sum of the diameters of all the holes. For example, the cut length perpendicular to the fiber
448 direction of the specimens with two holes of a diameter of 5 mm in the vertical direction (i.e.,
449 specimens H_n2d5_v50_h0_1/2) is equal to 10 mm. As a result, the reductions in compressive
450 strength and corresponding axial strain of specimens C_h50_1/2 are smaller than those of
451 specimens H_n2d5_v50_h0_1/2. The specimens with two holes of a larger diameter in the
452 vertical direction (e.g., specimens H_n2d8_v50_h0_1/2 with holes of a diameter of 8 mm) led to
453 a longer total cut length perpendicular to the fiber direction and thus the reductions in
454 compressive strength and corresponding axial strain are also larger.
455

456 **COMPARISON WITH JAWDHARI ET AL.'S (2021b) MODEL**

457 Jawdhari *et al*. (2021b) proposed a confinement model for FRP-wrapped circular concrete
458 columns subjected to damage of cut in the FRP wraps. The model was proposed for columns
459 confined with FRP wraps with fibers oriented only in the hoop direction. The reductions in
460 compressive strength and the corresponding axial strain caused by damage of cut in the FRP
461 wraps are reflected by the following two reduction parameters α and β, respectively:
462

$$\alpha = \left\{1.67 - 3.13\left(\frac{L_v}{L}\right) + 4.56\left(\frac{L_v}{L}\right)^2 - 2.14\left(\frac{L_v}{L}\right)^3 - 2.92\frac{y}{L} + 2.92\left(\frac{y}{L}\right)^2 + 0.0031f_c' - 0.0013E_f - 0.0563N\right\} \leq 1.0 \quad (1)$$

$$\beta = \left\{1.29 - 2.65\left(\frac{L_v}{L}\right) + 7.60\left(\frac{L_v}{L}\right)^2 - 4.20\left(\frac{L_v}{L}\right)^3 - 4.36\frac{y}{L} + 4.36\left(\frac{y}{L}\right)^2 + 0.0087\frac{D}{t_f}\right.$$

$$- 3.93 \times 10^{-5}\left(\frac{D}{t_f}\right)^2 + 4.45 \times 10^{-8}\left(\frac{D}{t_f}\right)^3 + 0.0145 f_c' - 0.0089 E_f \qquad (2)$$

$$\left. + 0.0474N + 1.49 \times 10^{-5}\left(\frac{E_f D}{t_f}\right)\right\} \leq 1.0$$

where L_v is the vertical cut length; L is the column height; y/L is the relative location of the center of the cut (= 0.5 for the specimens in the present study); D is the column concrete sectional diameter; E_f and t_f are the elastic modulus and the thickness of the FRP wrap; N is the number of cuts (= 1 for the specimens in the present study).

The above two reduction parameters α and β are incorporated into the following equations for the compressive strength and the corresponding axial strain in ACI 440.2R (2017):

$$\frac{f_{cc}'}{f_c'} = 1 + 3.3\left(\frac{\alpha f_l}{f_c'}\right) \qquad (3)$$

$$\frac{\varepsilon_{cc}}{\varepsilon_{co}} = 1.50 + 12\left(\frac{\varepsilon_{h,rup}}{\varepsilon_{co}}\right)^{0.45}\left(\frac{\beta f_l}{f_c'}\right) \qquad (4)$$

where $f_l = 2E_f t_f \varepsilon_{h,rup}/D$ is the confining pressure at FRP rupture; $\varepsilon_{h,rup}$ is the FRP hoop rupture strain which is taken as the average FRP hoop rupture strain obtained from the intact CFFT specimens in the present study (= 2.414%).

With Eqs. (1) to (4), the reduction ratios of the compressive strength and the corresponding axial strain (i.e., the ratio of the compressive strength or the corresponding axial strain of the specimen with tube damage and that of the corresponding intact specimen) of the test CFFT specimens

with a vertical cut can be predicted. Figure 15 shows the predictions of the strength reduction ratio and the strain reduction ratio versus the vertical cut length in comparison with the test results. It is interesting to observe that Jawdhari *et al*.'s (2021b) model slightly overestimates the strength reduction ratios of the test specimens, although the trend of the strength reduction ratio versus the vertical cut length is well captured by the model (Figure 15a). However, the strain reduction ratios are dramatically overestimated by Jawdhari *et al*.'s (2021b) model and the predicted trend of the strain reduction ratio versus the vertical cut length differ greatly to the test result. It is expected that as the vertical cut length increases, both the compressive strength and the corresponding axial strain reduce and approach the values of unconfined concrete. Therefore, the trend for the strain reduction ratio predicted by Jawdhari *et al*.'s (2021b) model may be incorrect. It should be noted again that Jawdhari *et al*.'s (2021b) model was proposed for FRP-wrapped concrete columns with fibers oriented only in the hoop direction and should be recalibrated in the future for CFFTs with a filament wound FRP tube. Such recalibration, however, requires more test data as well as results of detailed FE modelling of CFFTs with various parameters, which forms a future study of the authors.

CONCLUSIONS

This paper presents the results of an experimental program on concrete filled FRP tubular (CFFT) columns with a filament wound FRP tube subjected to local tube damage. Such local tube damage may be caused by accidental damage/vandalism or designed holes/cuts for various purposes. Two types of damage (i.e., holes and cuts) with different parameters were investigated. An existing model for FRP-confined concrete considering the local FRP damage was also evaluated using the test results of the presents study. The present study provided the much-

needed experimental data for the establishment of FE models and design methods in the future for CFFTs as columns with local FRP tube damage. Based on the test results and discussions presented in this paper, the following conclusions may be drawn:

1. The CFFT specimens with a horizontal cut failed in a process similar to those of the intact CFFT specimens; however, the total area of white patches and the final rupture sound of the former were smaller. The failure of the CFFT specimens with a vertical cut was initiated by outward buckling of the FRP tube near the cut, followed by fiber rupture near the two ends of the cut. The CFFT specimens with the damage of holes generally failed by explosive FRP rupture with fiber rupture being initiated around the holes. Compared with the control specimens, the specimens with the damage of holes failed with a more localized pattern.
2. The axial stress-axial strain curve of a CFFT specimen with local tube damage induced by a horizontal cut or holes features a bilinear shape before the peak stress, followed by a sudden axial stress drop due to FRP rupture with a descending branch. For the CFFT specimens with a small vertical cut, the axial stress-axial strain curve still features a bilinear shape; however, as the length of the cut increases, the axial stress-axial strain curve becomes more similar to that of unconfined concrete.
3. The compressive strengths and the corresponding axial strains of the CFFT specimens with local tube damage were significantly reduced compared with those of the intact specimens. The reductions in the compressive strength and the corresponding axial strain of the specimens with vertical cuts (40.0% and 55.1%, respectively for the compressive strength and the corresponding axial strain) were larger than those with horizontal cuts

(12.2% and 35.2%, respectively). The differences of CFFT specimens with different distances of holes, hole diameters, or numbers of holes (8.6% and 9.2%, respectively) were much smaller than those of the specimens with different cut directions or cut lengths (52.6% and 42.0%, respectively).

4. The compressive strengths of the CFFT specimens with a relatively large vertical cut (e.g., specimens C_v100 and C_v150) were close to that of unconfined concrete; however, the axial stress-axial strain curves of the damaged CFFT specimens exhibited a more gradual descending branch due to the confinement of the intact FRP tube near the two column ends.
5. The widely used method of clamping LVDTs onto a CFFT employing a test rig with screws may damage the FRP tube, resulting in a premature failure of the specimen. The methods without using screws, such as the use of epoxy mortar in the present study, are highly recommended for testing CFFTs with a filament wound FRP tube in the future.
6. Jawdhari *et al*.'s (2021b) model predicts the trend of the strength reduction ratio varying with the vertical cut length very well, although it slightly overestimates the strength reduction ratios of the test specimens. However, the strain reduction ratios of the test specimens are dramatically overestimated by the model and the predicted trend of the strain reduction ratio varying with the vertical cut length seems incorrect. Jawdhari *et al*.'s (2021b) model should be recalibrated for CFFTs with a filament wound FRP tube, which requires more test data as well as results of detailed FE modelling of CFFTs with various parameters in the future.
7. In the present study, all the test CFFTs had a filament wound FRP tube with a fiber angle of ±80°. However, the effects of tube damage on the behavior of CFFTs (including the

failure mode, stress-strain behavior, and ultimate condition) are sensitive to the fiber architecture of the FRP tube, as well as many other factors (e.g., tube diameter and concrete strength). As a result, the conclusions reached in the present study should be limited to CFFTs tested in the present study and more test data on CFFTs with wider ranges of parameters are needed before more solid and general conclusions can be reached.

DATA AVAILABILITY STATEMENT

All data, models, and code generated or used during the study appear in the submitted article.

ACKNOWLEDGEMENTS

The authors gratefully acknowledge the financial support provided by the National Natural Science Foundation of China (Project No.: 52008361) and the Hong Kong Research Grants Council (Project No: T22-502/18-R). They also wish to thank Mr. Ka-Hang Kwok for his valuable contribution to the experimental work.

NOTATION

The following symbols are used in the present paper.

f_c' = compressive strength (i.e., peak stress) of unconfined concrete;

f_{cc}' = compressive strength (i.e., peak stress) of FRP-confined concrete;

ε_c = axial strain of FRP-confined concrete;

ε_{co} = axial strain at peak stress of unconfined concrete;

ε_{cc} = axial strain at peak stress of FRP-confined concrete;

ε_{cu} = ultimate axial strain of FRP-confined concrete;

$\varepsilon_{h,rup}$ = average FRP hoop rupture strain;

L_h = length of a horizontal cut;

L_v = length of a vertical cut;

n = number of holes;

d = diameter of a hole;

w = horizontal distance between of two columns of holes;

H = vertical distance between two rows of holes;

L = height of a CFFT column;

D = concrete cross-sectional diameter;

y/L = relative location of the center of a cut;

E_f = elastic modulus of an FRP wrap;

t_f = thickness of an FRP wrap;

N = number of cuts;

α = reduction factor for f'_{cc};

β = reduction factor for ε_{cc}.

REFERENCES

AASHTO (2012). *LRFD Guide Specifications for Design of Concrete-Filled FRP Tubes for Flexural and Axial Members*. 1st ed., Washington, DC: AASHTO.

ACI 440.2R (2017). *Guide for the Design and Construction of Externally Bonded FRP Systems for Strengthening Concrete Structures*. American Concrete Institute, Farmington Hills, Michigan, USA.

571 Adheem, A. H., Kadhim, M. M., Jawdhari, A. and Fam, A. (2021). "Confinement model for
572 concrete wrapped with fiber reinforced cementitious mortar", *Construction and Building*
573 *Materials*, 312, 125401.
574 ASTM C469 (2022). *Standard Test Method for Static Modulus of Elasticity and Poisson's Ratio*
575 *of Concrete in Compression*. ASTM International, West Conshohocken, Pennsylvania,
576 USA.
577 ASTM D2290 (2019). *Standard Test Method for Apparent Hoop Tensile Strength of Plastic or*
578 *Reinforced Plastic Pipe by Split Disk Method*. ASTM International, West Conshohocken,
579 Pennsylvania, USA.
580 Burgueño, R. and Bhide, K.M. (2006). "Shear response of concrete-filled FRP composite
581 cylindrical shells", *Journal of Structural Engineering*, ASCE, Vol. 132, No. 6, pp. 949-
582 960.
583 Dong, Z., Han, T., Zhang, B., Zhu, H., Wu, G., Wei, Y. and Zhang, P. (2021). "A review of the
584 research and application progress of new types of concrete-filled FRP tubular members",
585 *Construction and Building Materials*, Vol. 312, pp. 125353.
586 Echevarria, A., Zaghi, A.E., Christenson, R. and Plank, R. (2015). "Residual axial capacity
587 comparison of CFFT and RC bridge columns after fire", *Polymers*, Vol. 7, No. 5, pp.
588 876-895.
589 El-Zefzafy, H., Mohamed, H.M. and Masmoudi, R. (2013). "Evaluation effects of the short-and
590 long-term freeze-thaw exposure on the axial behavior of concrete-filled glass fiber-
591 reinforced-polymer tubes", *Journal of Composites*, Vol. 2013, pp. 340672.
592 ElGawady, M.A. and Dawood, H.M. (2012). "Analysis of segmental piers consisted of concrete
593 filled FRP tubes", *Engineering Structures*, Vol. 38, pp. 142-152.

Fam, A., Greene, R. and Rizkalla, S. (2003a). "Field applications of concrete-filled FRP tubes for marine piles", *Special Publication*, Vol. 215, pp. 161-180.

Fam, A., Pando, M., Filz, G. and Rizkalla, S. (2003b). "Precast piles for Route 40 bridge in Virginia using concrete filled FRP tubes", *PCI Journal*, Vol. 48, No. 3, pp. 32-45.

Fam, A.Z. and Rizkalla, S.H. (2001a). "Behavior of axially loaded concrete-filled circular fiber-reinforced polymer tubes", *ACI Structural Journal*, Vol. 98, No. 3, pp. 280-289.

Fam, A.Z. and Rizkalla, S.H. (2001b). "Confinement model for axially loaded concrete confined by circular fiber-reinforced polymer tubes", *ACI Structural Journal*, Vol. 98, No. 4, pp. 451-461.

Gholampour, A. and Ozbakkaloglu, T. (2018). "Behavior of steel fiber-reinforced concrete-filled FRP tube columns: Experimental results and a finite element model", *Composite Structures*, Vol. 194, pp. 252-262.

Hassanli, R., Youssf, O., Vincent, T., Mills, J.E., Manalo, A. and Gravina, R. (2020). "Experimental study on compressive behavior of FRP-confined expansive rubberized concrete", *Journal of Composites for Construction*, ASCE, Vol. 24, No. 4, pp. 04020034.

Jawdhari, A., Fam, A., & Sadeghian, P. (2020). Modeling the nonlinear response of ±55 angle-ply GFRP tube used in CFFT applications. In: *Proceedings of the 8th International Conference on Advanced Composite Materials in Bridges and Structures*, Sherbrooke, Quebec, Canada, 18-20 August."

Jawdhari, A., Fam, A. and Noël, M. (2021a). "Design equation for concrete-filled FRP tubes in flexure including damage effects", *Engineering Structures*, Vol. 239, pp. 112267.

615 Jawdhari, A., Hadhood, A. and Fam, A. (2021b). “Confinement model for FRP-wrapped circular
616 columns when the wraps are subjected to damage”, *Construction and Building Materials*,
617 Vol. 275, pp. 122101.
618 Ji, G., Li, G., Li, X., Pang, S.-S. and Jones, R. (2008). “Experimental study of FRP tube encased
619 concrete cylinders exposed to fire”, *Composite Structures*, Vol. 85, No. 2, pp. 149-154.
620 Lu, C. and Fam, A. (2020). “The effect of tube damage on flexural strength of±55 angle-ply
621 concrete-filled FRP tubes”, *Construction and Building Materials*, Vol. 240, pp. 117948.
622 Lu, C., St. Onge, J. and Fam, A. (2020). “Damage threshold of near-cross-ply tubes used in
623 concrete-filled FRP tubes loaded in flexure”, *Journal of Composites for Construction*,
624 ASCE, Vol. 24, No. 2, pp. 04019063.
625 Mirmiran, A. and Shahawy, M. (1997). “Behavior of concrete columns confined by fiber
626 composites”, *Journal of Structural Engineering*, ASCE, Vol. 123, No. 5, pp. 583-590.
627 Ozbakkaloglu, T. and Oehlers, D.J. (2008). “Concrete-Filled Square and Rectangular FRP Tubes
628 under Axial Compression”, *Journal of Composites for Construction*, ASCE, Vol. 12, No.
629 4, pp. 469-477.
630 Qasrawi, Y., Heffernan, P.J. and Fam, A. (2015). “Performance of concrete-filled FRP tubes
631 under field close-in blast loading”, *Journal of Composites for Construction*, ASCE, Vol.
632 19, No. 4, pp. 04014067.
633 Robert, M. and Fam, A. (2012). “Long-term performance of GFRP tubes filled with concrete and
634 subjected to salt solution”, *Journal of Composites for Construction*, ASCE, Vol. 16, No.
635 2, pp. 217-224.

636 Rodsin, K., Hussain, Q., Suparp, S. and Nawaz, A. (2020). “Compressive behavior of extremely
637 low strength concrete confined with low-cost glass FRP composites”, *Case Studies in*
638 *Construction Materials*, Vol. 13, pp. e00452.
639 Shi, Y., Li, B. and Mirmiran, A. (2011). “Combined shear and flexural behavior of hybrid FRP-
640 concrete beams previously subjected to cyclic loading”, *Journal of Composites for*
641 *Construction*, ASCE, Vol. 15, No. 5, pp. 841-849.
642 Taveras, O., Fam, A., Hadhood, A., and Song, B. K. (2022). Experimental investigation of axial
643 strength of damaged concrete-filled FRP tubes. *Structures*, Vol. 44, pp. 1783-1796.
644 Tejada, O. D. T. (2021). *Experimental Assessment of FRP-Confined Concrete Columns with*
645 *Damaged Jackets*, MSc Thesis, Queen's University, Canada.
646 Teng, J.G., Yu, T., Wong, Y.L. and Dong, S.L. (2007). “Hybrid FRP-concrete-steel tubular
647 columns: concept and behavior”, *Construction and Building Materials*, Vol. 21, No. 4, pp.
648 846-854.
649 Tijani, I.A., Jiang, C., Lim, C. and Wu, Y.-F. (2020). “Effect of load eccentricity on the
650 mechanical response of FRP-confined predamaged concrete under compression”, *Journal*
651 *of Composites for Construction*, ASCE, Vol. 24, No. 5, pp. 04020057.
652 Vincent, T. and Ozbakkaloglu, T. (2013). “Influence of fiber orientation and specimen end
653 condition on axial compressive behavior of FRP-confined concrete”, *Construction and*
654 *Building materials*, Vol. 47, pp. 814-826.
655 Wang, S. and ElGawady, M.A. (2020). “Performance of concrete-filled fiber-reinforced polymer
656 tube stubs subjected to sustained axial load and long-term seawater corrosion”, *ACI*
657 *Materials Journal*, Vol. 117, No. 5, pp. 13-26.

658 Yu, T. and Teng, J.G. (2011). “Design of concrete-filled FRP tubular columns: provisions in the
659 Chinese technical code for infrastructure application of FRP composites”, *Journal of*
660 *Composites for Construction*, ASCE, Vol. 15, No. 3, pp. 451-461.
661 Yu, T., Zhang, B. and Teng, J.G. (2015). “Unified cyclic stress–strain model for normal and high
662 strength concrete confined with FRP”, *Engineering Structures*, Vol. 102, pp. 189-201.
663 Zhang, B., Teng, J.G. and Yu, T. (2017). “Compressive behavior of double-skin tubular columns
664 with high-strength concrete and a filament-wound FRP tube”, *Journal of Composites for*
665 *Construction*, ASCE, Vol. 21, No. 5, pp. 04017029.
666 Zhang, B., Yu, T. and Teng, J.G. (2015). “Behavior of concrete-filled FRP tubes under cyclic
667 axial compression”, *Journal of Composites for Construction*, ASCE, Vol. 19, No. 3, pp.
668 04014060.
669 Zhu, Z., Ahmad, I. and Mirmiran, A. (2006). “Fiber element modeling for seismic performance
670 of bridge columns made of concrete-filled FRP tubes”, *Engineering Structures*, Vol. 28,
671 No. 14, pp. 2023-2035.
672 Zohrevand, P. and Mirmiran, A. (2013). “Seismic response of ultra-high performance concrete-
673 filled FRP tube columns”, *Journal of Earthquake Engineering*, Vol. 17, No. 1, pp. 155-
674 170.

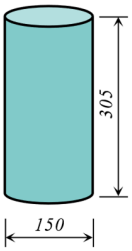

(a) Group A: tube without damage

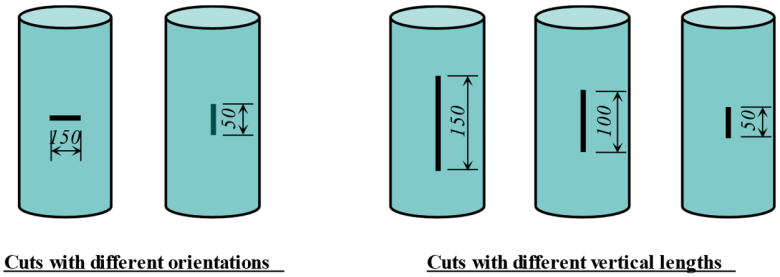

(b) Group B: tube damage induced by cutting

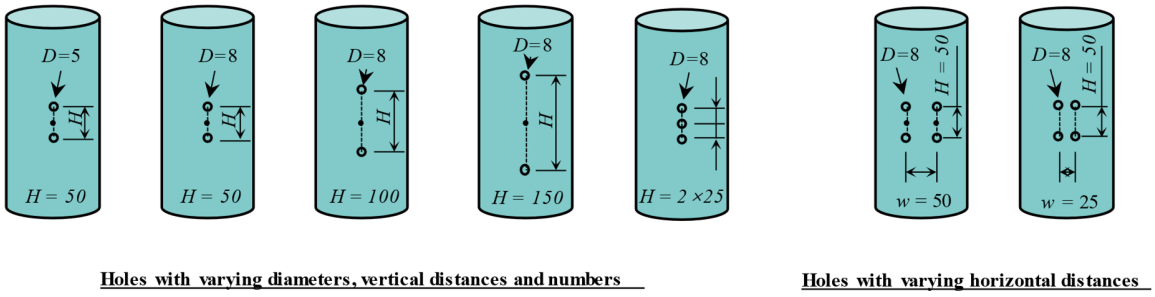

(c) Group C: tube damage induced by drilling holes

Figure 1. Schematic of the artificially induced local damage on the filament wound FRP tubes (units in mm).

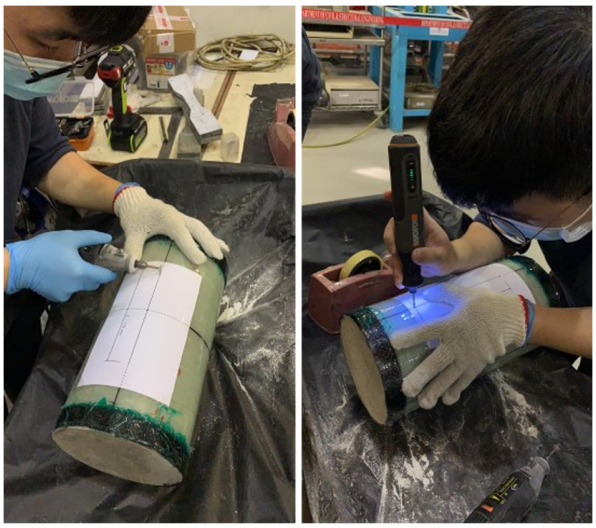

(a) **(b)**

Figure 2. Inducing local damage on FRP tubes by: (a) cutting; and (b) drilling.

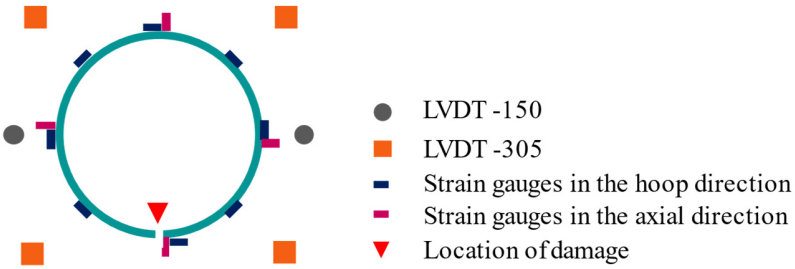

(a)

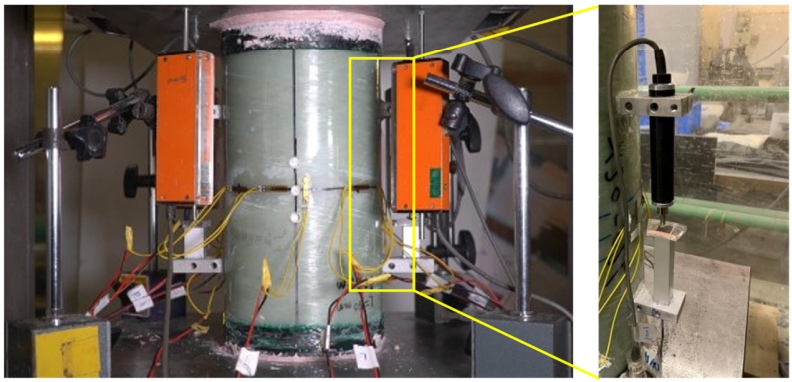

(b)

Figure 3. Test set-up and instrumentation: (a) layout of strain gauges and LVDTs; and (b) installation of LVDTs

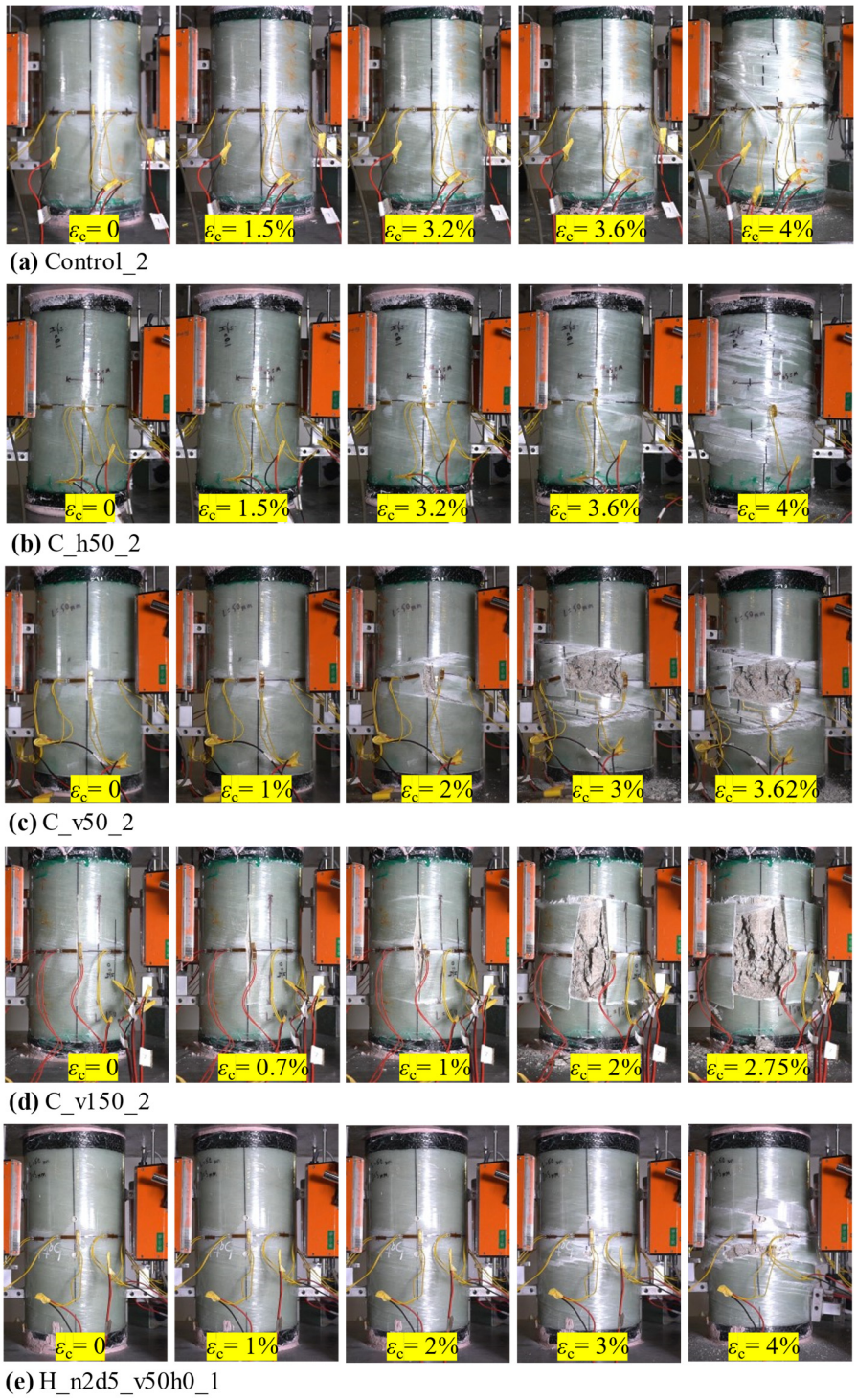

Figure 4. Typical failure process of specimens: (a) Control; (b) C_h50; (c) C_v50; (d) C_v150; (e) H_n2d5_v50h0; (f) H_n2d8_v50h0; (g) H_n2d8_v150h0; (h) H_n3d8_v50h0; (i) H_n4d8_v50h25; and (j) H_n4d8_v50h50.

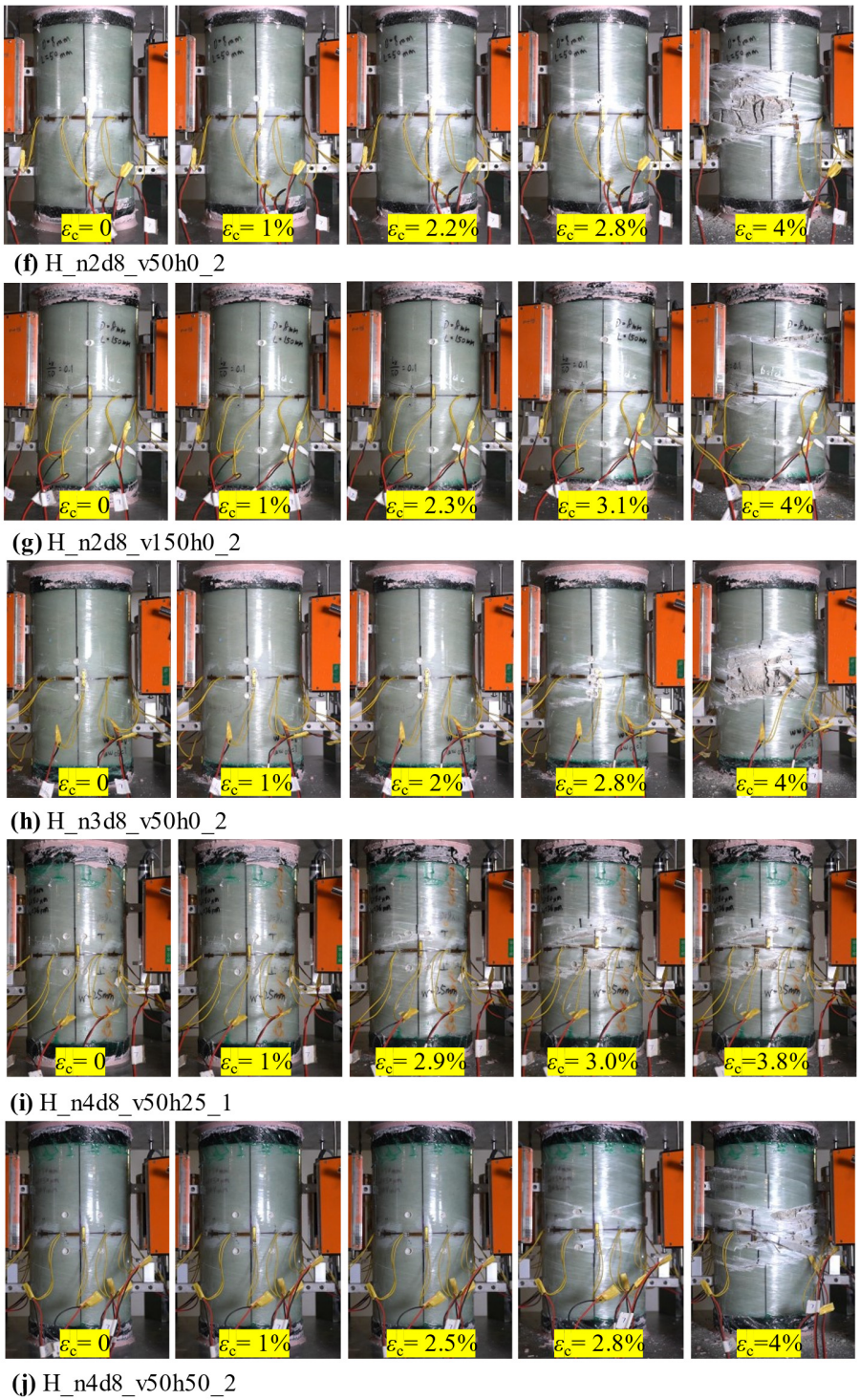

Figure 4. Typical failure process of specimens: (a) Control; (b) C_h50; (c) C_v50; (d) C_v150; (e) H_n2d5_v50h0; (f) H_n2d8_v50h0; (g) H_n2d8_v150h0; (h) H_n3d8_v50h0; (i) H_n4d8_v50h25; and (j) H_n4d8_v50h50. **(Cont.)**

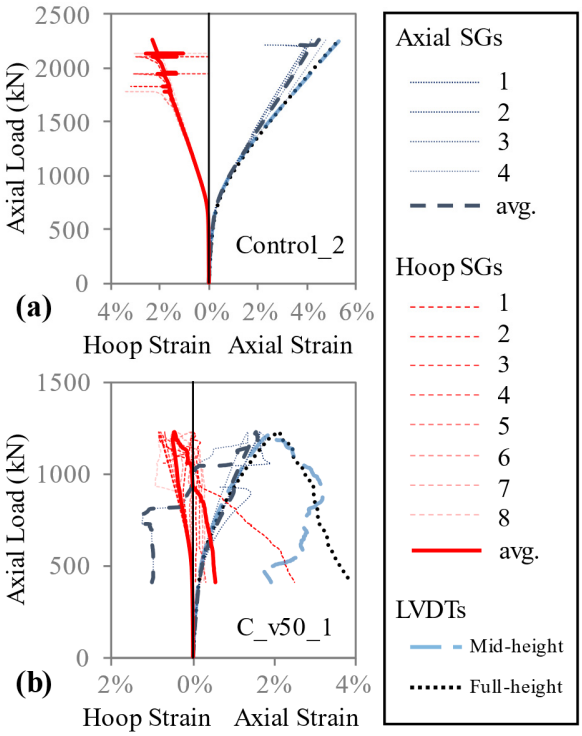

Figure 5. Typical experimental axial load-strain curves: (a) Specimen Control_2; and (b) Specimen C_v50_1.

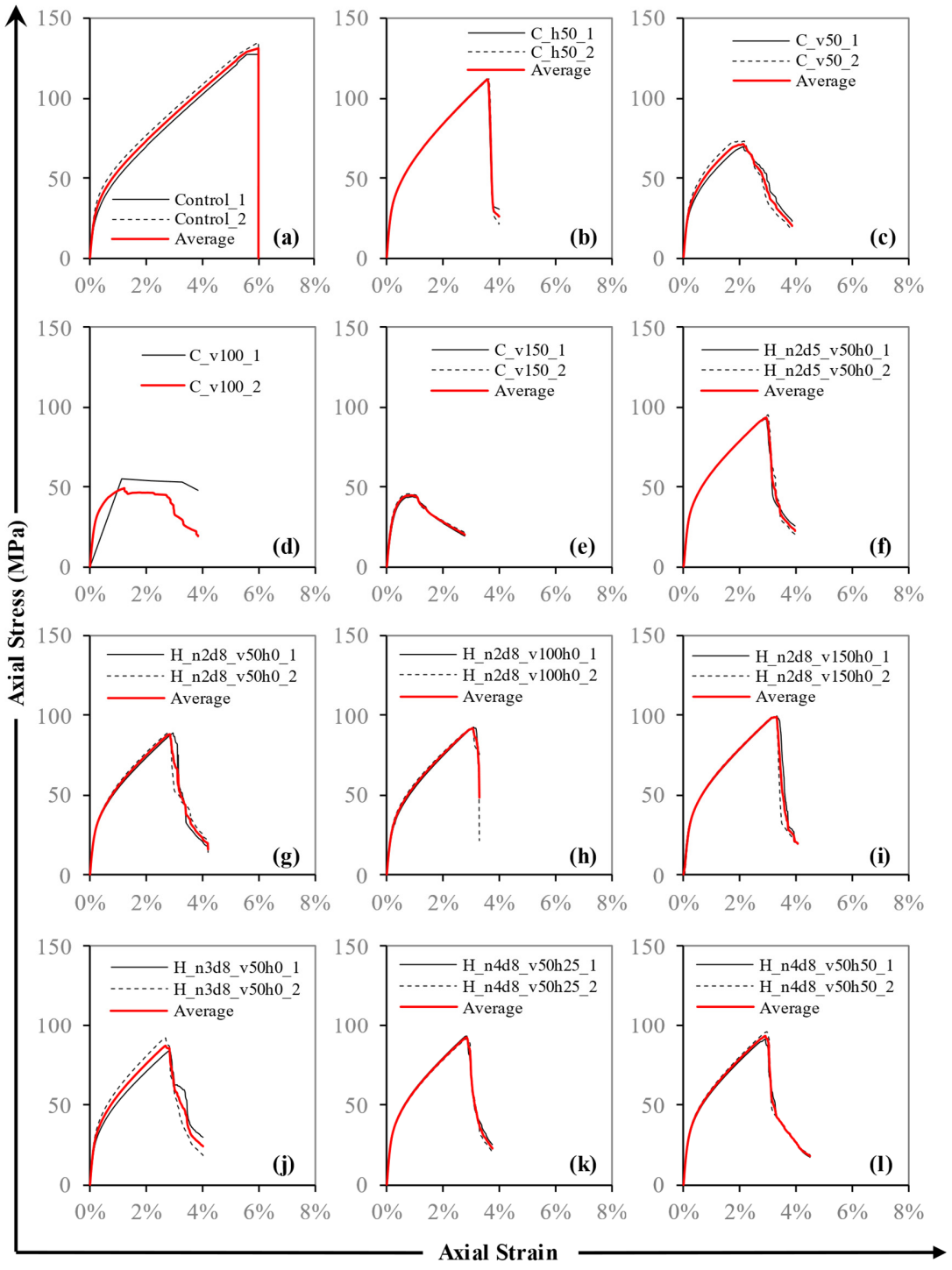

Figure 6. Axial stress-axial strain curves of specimens: (a) Control; (b) C_h50; (c) C_v50; (d) C_v100; (e) C_v150; (f) H_n2d5_v50h0; (g) H_n2d8_v50h0; (h) H_n2d8_v100h0; (i) H_n2d8_v150h0; (j) H_n3d8_v50h0; (k) H_n4d8_v50h25; and (l) H_n4d8_v50h50.

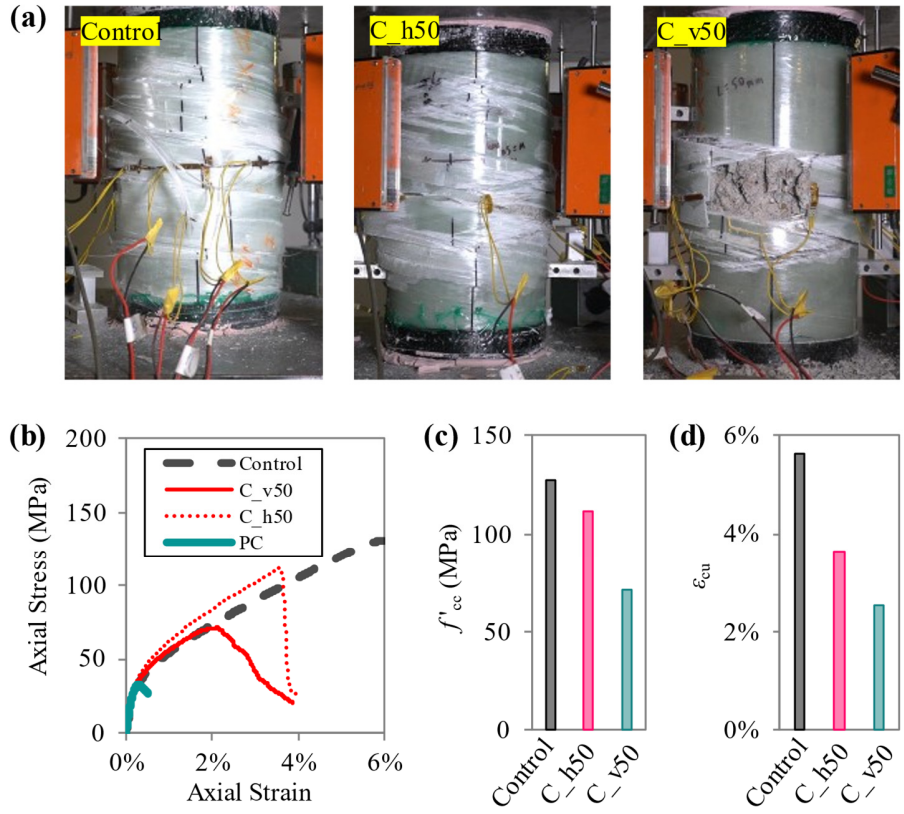

Figure 7. Comparisons of (a) failure patterns; (b) axial stress-axial strain curves; (c) ultimate axial stresses; and (d) ultimate axial strains of the specimens with different cutting directions.

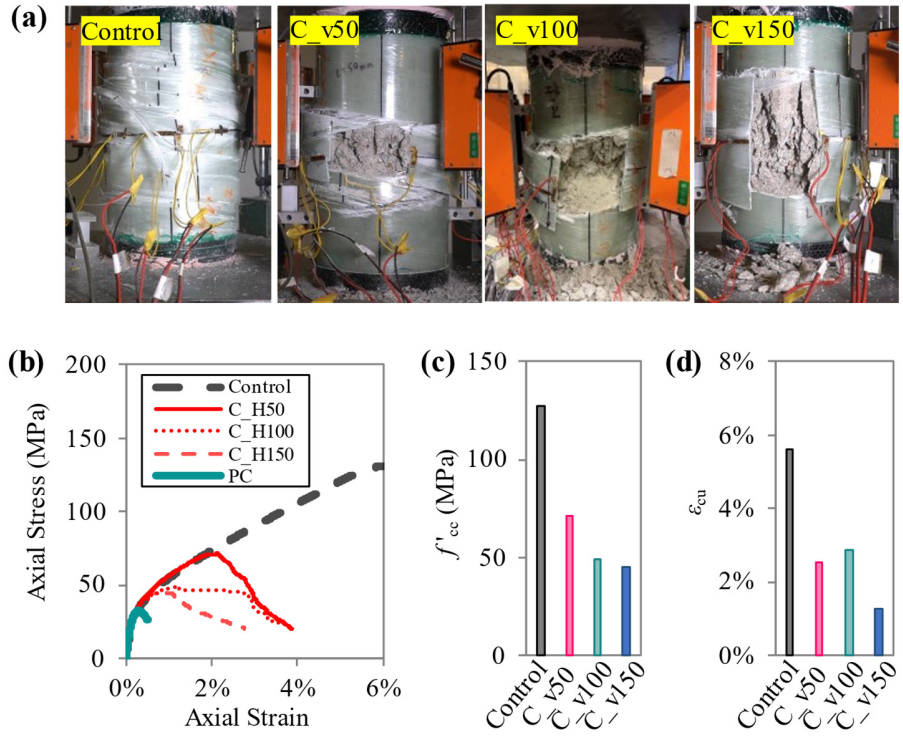

Figure 8. Comparisons of (a) failure patterns; (b) axial stress-axial strain curves; (c) ultimate axial stresses; and (d) ultimate axial strains of the specimens with different vertical cut lengths.

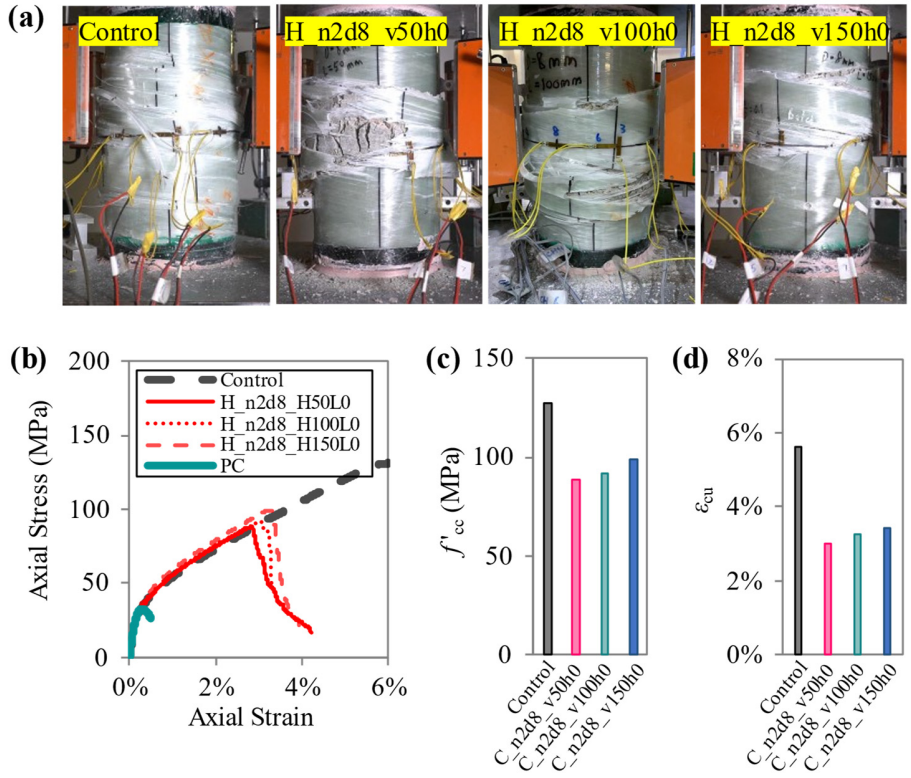

Figure 9. Comparisons of (a) failure patterns; (b) axial stress-axial strain curves; (c) ultimate axial stresses; and (d) ultimate axial strains of the specimens with holes of different vertical distances.

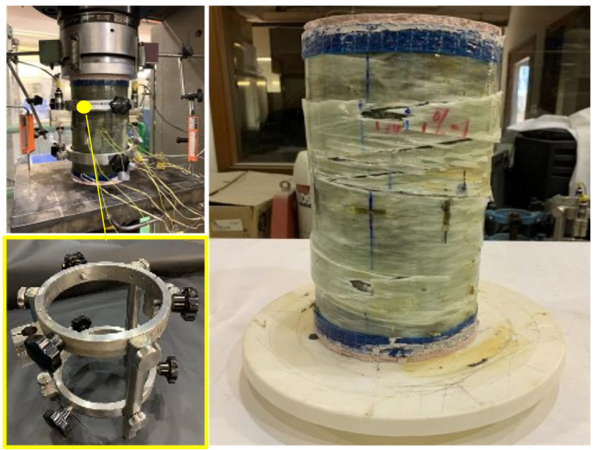

(a) (b)

Figure 10. A CFFT column with a screw-type test rig for clamping LVDTs tested previously by the authors' group: (a) test set-up; and (b) specimen failure mode.

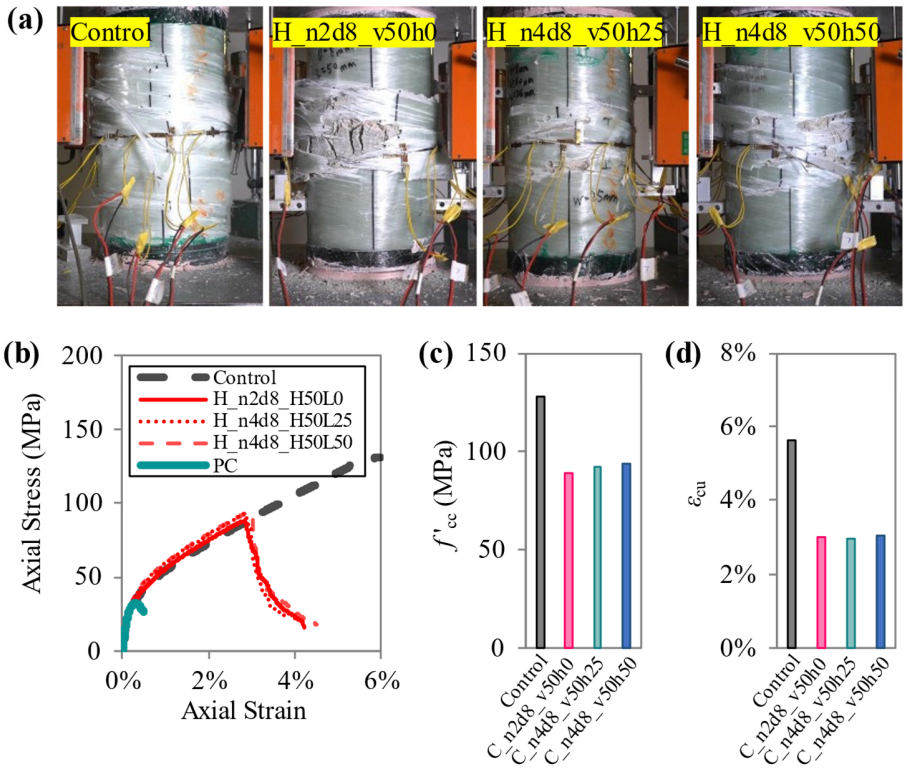

Figure 11. Comparisons of (a) failure patterns; (b) axial stress-axial strain curves; (c) ultimate axial stresses; and (d) ultimate axial strains of the specimens with different horizontal distances between two columns of holes.

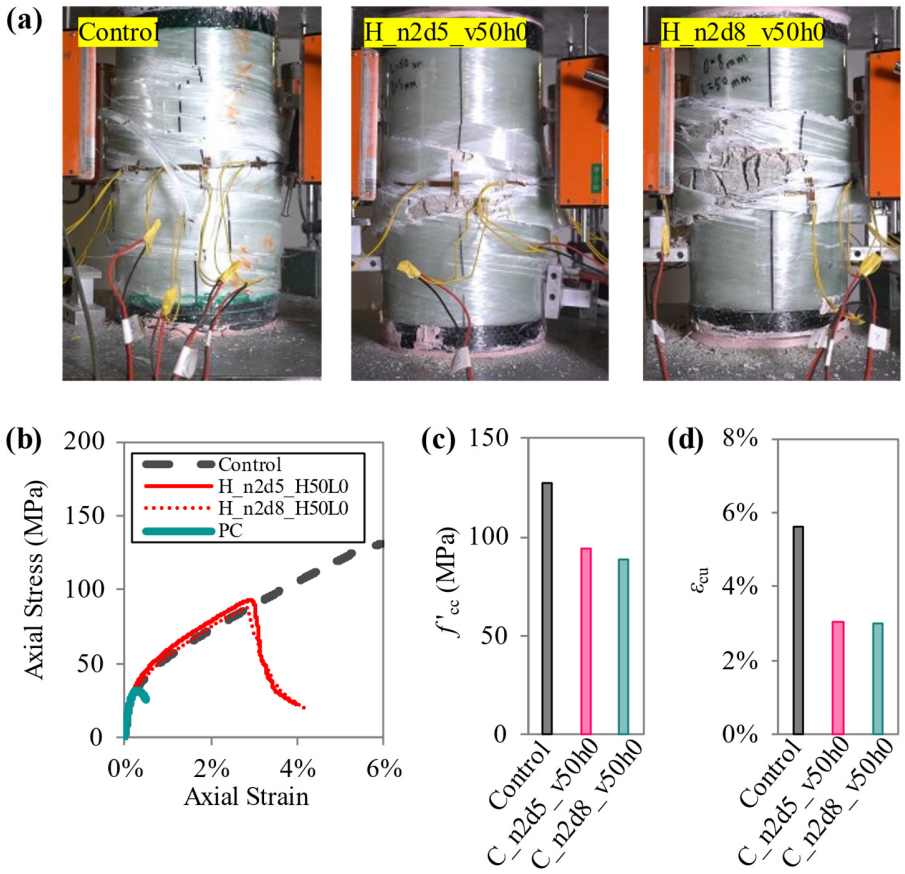

Figure 12. Comparisons of (a) failure modes; (b) axial stress-axial strain curves; (c) ultimate axial stresses; and (d) ultimate axial strains of the specimens with different hole diameters.

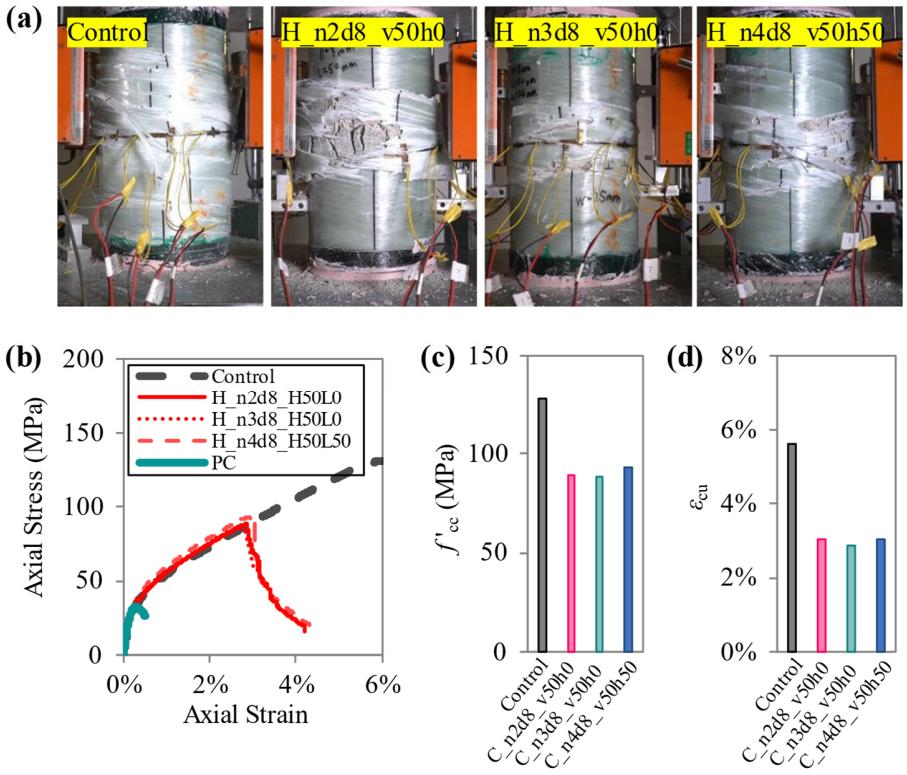

Figure 13. Comparisons of (a) failure modes; (b) axial stress-axial strain curves; (c) ultimate axial stresses; and (d) ultimate axial strains of the specimens with different numbers of holes.

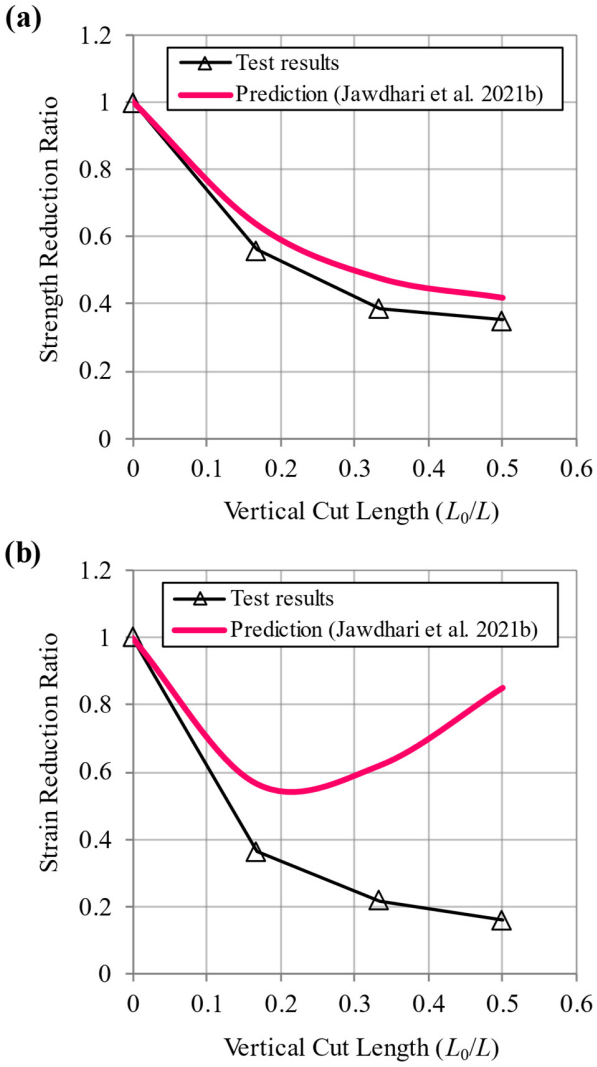

Figure 14. Comparisons of model predictions and experimental results on: (a) strength reduction ratio; and (b) strain reduction ratio for specimens with a vertical cut.

Table 1. Specimen details.

No	Group	Specimen	Damage Pattern
1	A: Control	Control_1	--
2		Control_2	--
3	B: Cut	C_h50_1	Horizontal cut of 50 mm length
4		C_h50_2	
5		C_v50_1	Vertical cut of 50 mm length
6		C_v50_2	
7		C_v100_1	Vertical cut of 100 mm length
8		C_v100_2	
9		C_v150_1	Vertical cut of 150 mm length
10		C_v150_2	
11	C: Holes	H_n2d5_v50h0_1	Two 5 mm holes with a vertical distance of 50 mm
12		H_n2d5_v50h0_2	
13		H_n2d8_v50h0_1	Two 8 mm holes with a vertical distance of 50 mm
14		H_n2d8_v50h0_2	
15		H_n2d8_v100h0_1	Two 8 mm holes with a vertical distance of 100 mm
16		H_n2d8_v100h0_2	
17		H_n2d8_v150h0_1	Two 8 mm holes with a vertical distance of 150 mm
18		H_n2d8_v150h0_2	
19		H_n3d8_v50h0_1	Three 8 mm holes with a vertical distance of 50 mm
20		H_n3d8_v50h0_2	
21		H_n4d8_v50h25_1	Four 8 mm holes with a vertical and horizontal distances of 50 mm and 25 mm
22		H_n4d8_v50h25_2	
23		H_n4d8_v50h50_1	Four 8 mm holes with a vertical and horizontal distances of 50 mm and 50 mm
24		H_n4d8_v50h50_2	

Table 2. Key results of test specimens.

Specimen	f'_{cc} (MPa)	Average f'_{cc} (MPa)	ε_{cc}	Average ε_{cc}	ε_{cu}	Average ε_{cu}	$\varepsilon_{h,rup}$	Average $\varepsilon_{h,rup}$
Control_1	127.3	127.6	5.929%	5.628%	5.929%	5.628%	2.520%	2.414%
Control_2	127.9		5.328%		5.328%		2.308%	
C_h50_1	112.0	112.0	3.570%	3.601%	3.620%	3.650%	1.029%	0.798%
C_h50_2	112.0		3.631%		3.681%		0.567%	
C_v50_1	69.54	71.41	2.116%	2.036%	2.615%	2.527%	0.459%	0.476%
C_v50_2	73.28		1.957%		2.439%		0.493%	
C_v100_1*	-	49.38	-	1.221%	-	2.859%	-	0.317%
C_v100_2	49.38		1.221%		2.859%		0.317%	
C_v150_1	44.08	44.97	0.921%	0.894%	1.396%	1.283%	0.193%	0.177%
C_v150_2	45.85		0.867%		1.170%		0.162%	
h_n2d5_v50h0_1	92.59	93.94	2.932%	2.967%	3.025%	3.057%	1.393%	1.412%
h_n2d5_v50h0_2	95.29		3.002%		3.089%		1.432%	
H_n2d8_v50h0_1	88.89	88.99	2.952%	2.868%	3.139%	3.022%	1.390%	1.249%
H_n2d8_v50h0_2	89.09		2.783%		2.904%		1.109%	
H_n2d8_v100h0_1	92.57	92.03	3.091%	3.066%	3.254%	3.244%	1.372%	1.349%
H_n2d8_v100h0_2	91.49		3.040%		3.234%		1.326%	
H_n2d8_v150h0_1	99.48	99.09	3.323%	3.232%	3.475%	3.411%	1.689%	1.607%
H_n2d8_v150h0_2	98.70		3.140%		3.348%		1.524%	
H_n3d8_v50h0_1	84.31	88.18	2.825%	2.755%	2.933%	2.891%	1.091%	1.065%
H_n3d8_v50h0_2	92.04		2.684%		2.849%		1.038%	
H_n4d8_v50h25_1	93.20	92.36	2.843%	2.834%	2.958%	2.973%	1.144%	1.221%
H_n4d8_v50h25_2	91.53		2.826%		2.987%		1.298%	
H_n4d8_v50h50_1	91.19	93.52	2.901%	2.937%	3.025%	3.039%	1.169%	1.249%
H_n4d8_v50h50_2	95.84		2.973%		3.054%		1.328%	

Note: *Specimen C_v100_1 was failed due to an operational error; therefore, its results are excluded from averaging.